NASA TECHNICAL NOTE

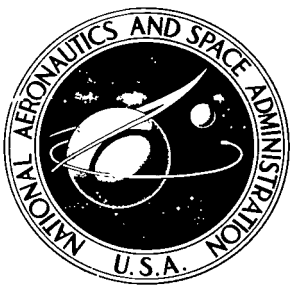

NASA TN D-4506

METHOD AND RESULTS OF STUDYING VAPOR DEPOSITION NUCLEATION PROCESSES BY IN SITU ELECTRON MICROSCOPY

by Helmut Poppa

Ames Research Center
Moffett Field, Calif.

NATIONAL AERONAUTICS AND SPACE ADMINISTRATION • WASHINGTON, D. C. • APRIL 1968

METHOD AND RESULTS OF STUDYING VAPOR DEPOSITION NUCLEATION PROCESSES BY IN SITU ELECTRON MICROSCOPY

By Helmut Poppa

Ames Research Center
Moffett Field, Calif.

NATIONAL AERONAUTICS AND SPACE ADMINISTRATION

For sale by the Clearinghouse for Federal Scientific and Technical Information
Springfield, Virginia 22151 – CFSTI price $3.00

METHOD AND RESULTS OF STUDYING VAPOR DEPOSITION NUCLEATION PROCESSES BY IN SITU ELECTRON MICROSCOPY*

By Helmut Poppa

Ames Research Center

SUMMARY

The kinetics of nucleation in some simple substrate-overgrowth systems have been measured quantitatively by improved in situ electron microscopy techniques. The nucleation of bismuth and silver on evaporated carbon and the nucleation of bismuth on evaporated SiO substrates were studied as a function of substrate temperature and impinging flux. The results were analyzed in terms of the phenomenological theory of nucleation and in terms of Walton's atomistic model of condensation from the vapor phase. Both theoretical concepts led to specific conclusions concerning such nucleation parameters as the number of atoms in the critical nucleus n^* and the free energy of desorption ΔG_{des}. The substrate temperature and impingement flux dependence of the maximum number of particles deposited on the substrate surface were determined and tentatively interpreted on the basis of nucleation limited surface migration. Some nucleation induction time observations were made and were related to the clustering kinetics of adatoms, the growth process of individual nuclei, and the instrument limitations of the detection method.

INTRODUCTION

The study of kinetics and elementary processes in the deposition of materials from the vapor phase onto solid surfaces is closely associated with the general problem of phase and order transitions. Phase change phenomena, of wide interest in physics and chemistry, have the nucleation process as a common denominator. Nucleation investigations are spurred by the growing need for new knowledge in such fields as (1) the corrosion of metals; (2) solidification, crystallization, and precipitation in metal foils; and (3) the structure and properties of metal, semiconductor, and dielectric thin films produced by evaporation, chemical vapor decomposition, sputtering, and electrodeposition. Since early theoretical work (refs. 1-3), most investigations (see Hirth and Pound's comprehensive review, ref. 4) have explored the theoretical aspects of homogeneous nucleation.

---

*The experimental part of this work was performed at the Space Science Laboratories of General Dynamics/Convair, San Diego, California. The analytical part of this investigation was accomplished while the author held a National Research Council Postdoctoral Resident Research Associateship supported by the NASA-Ames Research Center, Moffett Field, California.

Relatively few experimental studies of heterogeneous nucleation are sufficiently reliable to permit comparisons with theoretical predictions (refs. 4-9). The necessity for providing better control of the most important experimental parameters is now generally recognized, and has led to some meaningful quantitative deposition studies (refs. 10-13). Still, the situation is characterized by a lack of reliable experimental data. Hirth and Pound (ref. 4) state: "In view of the scarcity of significant quantitative data in this field, it would seem that almost any critical supersaturation measurements in which crystallographic orientation, degree of imperfection, and extent of contamination of the substrate are known and controlled should be most fruitful."

The current investigation was undertaken to obtain nucleation data on overgrowth-substrate combinations Bi on C (amorph.), Bi on SiO (amorph.), and Ag on C (amorph.). The results are compared with two theoretical approaches to the heterogeneous nucleation problem. It was intended to determine, through comparative studies, whether the nucleation processes in the simple systems would be described adequately either by Walton's statistical theory of condensation (ref. 14) or by the Volmer-Becker-Pound phenomenological approach (ref. 4). It was hoped that the experience acquired with simple deposition systems might then aid in applying the same principles to more complex vapor depositions on substrates.

The author is indebted to Professor G. M. Pound and Dr. E. Bauer for critical discussions, and to J. Dancy for able technical assistance in the experimental part of this study.

SYMBOLS

a_o	surface diffusion jump distance
c_v	volume growth velocity of deposit particle
D	diameter of growing deposit particle
d_s	root mean square (rms) surface diffusion distance
E_{n^*}	dissociation energy of a critical nucleus containing n^* atoms
I	nucleation rate
l	Tolman parameter
N	impinging flux of deposit material at the substrate surface
$\tilde{N}$	experimental average of impinging flux N
N_{n^*}	number density of critical nuclei
n	number density of deposit particles

n^*	number of atoms or molecules in the critical nucleus
n_{max}	maximum number density of growing deposit particles
n_o	number density of nucleation sites
n_s	adatom population
p	vapor pressure ($N\sqrt{2\pi mkt}$)
p_e	equilibrium vapor pressure
p_t	total residual gas pressure
S	supersaturation ratio, p/p_e
T	substrate temperature
T_m	melting temperature of deposit material
t_i	time from formation of fresh surface to initiation of electron beam influence
t_m	time for monolayer adsorption
t_o	$t_1 + t_2 + t_3 + t_4$ = total time lag for detection of nuclei
t_1	time needed to build up an equilibrium concentration of adatoms on the substrate surface
t_2	time required to establish a steady-state distribution of clusters of subcritical size, assuming a starting point with constant p/p_e
t_3	time required by a single growing nucleus to reach observable size
t_4	detection time of particle in restricted field of view
V^o	volume of single growing deposit particle
α, β	shape factors accounting for varying particle geometry
γ	sticking coefficient of gases on substrate surface
ΔG^*	free energy of formation of the critical nucleus at rest
ΔG_{des}	Gibbs' free energy of desorption
ΔG_q	free energy change accompanying distribution of nuclei on a substrate surface with n_o adsorption sites

$\Delta G_r, \Delta G_t$	free energy change accompanying the activation of rotational (r) or translational (t) degrees of freedom
ΔG_{sd}	Gibbs' free energy of surface diffusion
θ	contact angle of condensed particle with substrate surface
σ_B	bulk surface tension
τ	time for surface diffusion
τ_s	mean residence time of an adatom
Φ	$\ln(p/p_e)$
φ_s	$(2 - 3 \cos \theta + \cos^3 \theta)/4$
Ω	molecular volume
ω	surface vibration frequency

NUCLEATION EXPERIMENTS

Method of Investigation and Limitations

It is difficult to conduct quantitative heterogeneous nucleation experiments because the important experimental nucleation parameters have to be well defined. Requirements are particularly critical for (1) the state of surface cleanliness of the substrate, and (2) the detection of small clusters of condensed atoms.

The first requirement is hardest to fulfill because the general knowledge on the structure of clean surfaces is quite limited and partly even controversial at present. However, low-energy electron diffraction (LEED) studies have shown unequivocally that extreme care is required in the preparation of clean surfaces and that ultra high vacuum (UHV) techniques providing pressures smaller than 10^{-6} torr are an absolute prerequisite.

The second requirement poses serious experimental difficulties too since extremely small nuclei must be detected if kinetic details of nucleation are to be studied and distinguished from later growth and coalescence processes. Current theoretical estimates of the number of atoms in the critical nucleus range from $n^* = 1$ (statistical theory) to several hundred (thermodynamical theory); thus, entities of atomic or near-atomic dimensions must be spotted. (Field ion and conventional high-resolution electron-microscopy methods both have the required resolving power and have therefore been used in recent quantitative nucleation studies (refs. 11 and 15).)

Serious complications are encountered when the experimental method involves combining a well-defined nucleation system with a microscopic method

of detection (ref. 16). High-resolution in situ electron microscopy can meet the requirements for reliable heterogeneous nucleation investigations if the method is adjusted so that one is able to:

1. Prepare clean surfaces with well-defined structure and properties. This condition is the hardest to attain during in situ microscopy. Cleavage in the available space seems impossible, and the chances for incorporating ion-bombardment cleaning provisions are small. However, heat cleaning and deposition of freshly evaporated surface layers are sufficient for certain substrate-overgrowth combinations.

2. Maintain a clean substrate or one covered with known amounts of adsorbed gases. Although complex in design, an UHV environment can be provided at the site of the electron microscopy specimen, or possibly in the entire microscope. Significant advances over earlier in situ work (refs. 17-19) have been made by employing differential pumping principles at the site of the specimen (refs. 15, 20, and 21).

3. Minimize the effects of the imaging electron beam. (Here the interaction of the beam with the substrate, the deposit, and the residual gases have to be considered.) These effects can be largely eliminated by combining lower background pressures, high substrate temperatures, and drastically reduced electron beam currents.[1]

4. Control and measure the impingement flux of the depositing material.

5. Measure the substrate temperature in the limited working space available in the electron microscope.

[1]It is worthwhile pointing out that intensification of the electron microscope (EM) image would greatly reduce electron beam intensities. In addition, an electronic intensification system with cathode-ray tube output offers other important advantages for detailed analysis: (1) "instant motion pictures" through video tape recording, and (2) instantaneous quantitative determination of number densities or size distributions of nuclei through electronic particles analysis with a flying spot system. An EM intensifier was not used, however, in the present experiments because the required equipment was not yet available.

Instrumentation and Experimental Procedures

The experimental arrangement (fig. 1) and techniques used for the quantitative in-situ nucleation experiments were essentially as described previously (ref. 15), except that the evaporation unit was modified to permit incorporation of a second evaporation source. The additional source could be used interchangeably with and was heated and rate checked independently of the first evaporation source. Each source could be moved quickly into a well-alined evaporation position by a mechanical drive mechanism. A fresh layer of a suitable substrate material could thus be deposited on a thin electron-microscope support film just before the start of nucleation of the overgrowth material.

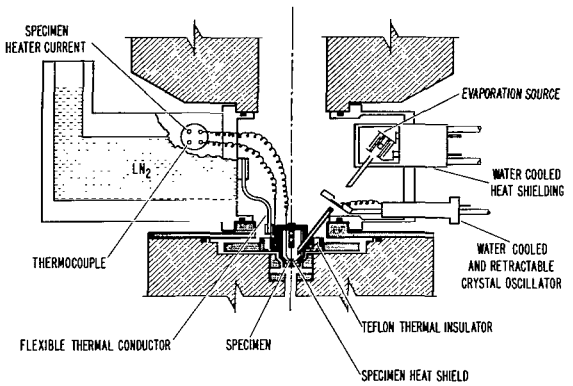

Figure 1.- Electron microscope specimen chamber.

The procedure for a typical nucleation test was as follows:

1. The carbon support film mounted on the platinum electron-microscope specimen-support grid was subjected to a high-temperature (800° C) cleaning treatment for about 10 min.

2. Both evaporation sources were outgassed simultaneously and the anticipated evaporation rates adjusted approximately.

3. The desired deposition temperature of the substrate was established while the operator was selecting and photographing a certain area of the substrate.

4. Before the chosen substrate material was deposited, the impinging flux of the overgrowth material to be used later during the nucleation experiment was accurately measured with the quartz crystal oscillator. Very small impingement fluxes, from 2×10^{13} to 3×10^{14} cm^{-2} sec^{-1}, were used at the site of the substrate.

5. The nucleation test began immediately after[2] the substrate film was deposited. Sometimes the substrate was again photographed and the impinging flux rechecked between the two depositions.

[2]The minimum delay between depositions was of the order of 1 sec. This could be achieved, however, only when both depositions were carried out at the same (usually high) substrate temperature. The first deposition had to be at a high rate and of short duration in order to form a thin and continuous substrate layer.

6. The electron microscope image was recorded at appropriate intervals during the nucleation and growth process. The built-in plate camera (36 exposures) was used whenever possible. Figure 2 is taken from a typical series of electron micrographs of an identical substrate area.

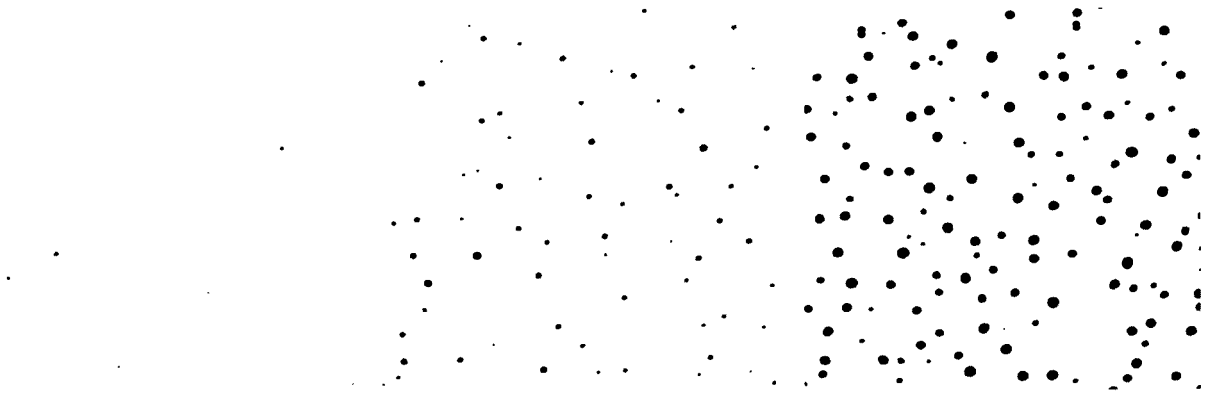

Figure 2.- Early stages of deposition during the nucleation of bismuth on an evaporated carbon substrate; 120,000X.

7. If changes in the microscope image were too rapid, motion-picture recording techniques were employed.

8. The nucleation experiment was usually terminated when merger processes of formerly separated deposit particles were observed.

9. The impinging flux of the nucleating material was measured again and compared with the flux measurement before the start of nucleation.

10. The photographs of nucleation and growth processes were evaluated with a manually operated Zeiss particle size analyzer to determine the sizes and number densities of particles.

Control and Measurement Accuracies of Important Nucleation Parameters

The test procedure and facilities did not permit continuous monitoring of the impinging flux of depositing material. The consequent errors in flux measurements is a principal source of experimental error in the quantitative nucleation experiments reported here. The evaporation sources were heated by thermal radiation, and changes in the evaporation rate were less than 8 percent over periods of up to 15 min. To achieve such long-term evaporation stability without employing feedback loops, transistor-regulated direct-current power supplies were used.

A highly accurate substrate temperature measurement is desirable because, next to the impingement flux, the substrate temperature is the most important experimental variable. The substrate heater was calibrated carefully to insure reproducible results; the relative temperature measurements are considered accurate within 1 to 2 percent.

The total residual gas pressure at the site of the electron-microscope substrate specimen had been measured directly (see ref. 15). A second

evaporation source provided an independent way of checking the direct measurements through nucleation measurements. The density of deposited particles, and therefore the nucleation rate, is always appreciably higher in that area of a carbon substrate where the illuminating electron beam intercepts the substrate during bismuth deposition. This effect has been tentatively explained (ref. 15) by the capacity of the electron beam to desorb gases from the substrate surface and thereby increase the nucleation potency of the substrate. It should be possible, therefore, to accomplish bismuth nucleation without preferred nucleation in the electron-beam area for the time that the substrate stays relatively clean after a freshly evaporated carbon substrate is formed. This period should be of the same order of magnitude as that needed to adsorb a monolayer of residual gases. A series of nucleation runs was conducted during which bismuth deposition was started at various times after deposition of a fresh carbon substrate was terminated. These runs proved that for time lags up to 120 sec, no beam influence can be detected. If the time lags are taken as approximately equal to the time of monolayer adsorption, values for the partial pressure of active residual gases that affect the nucleation rate can be deduced (fig. 3). Depending upon the sticking coefficient γ, pressure values ranging from 1.5×10^{-8} to 1.5×10^{-7} torr are obtained and agree well with previous estimates (ref. 15). Because of the low residual gas pressure and limitation to simple nucleation systems, the influence of the imaging electron beam on the processes under study was reduced to negligible proportions.

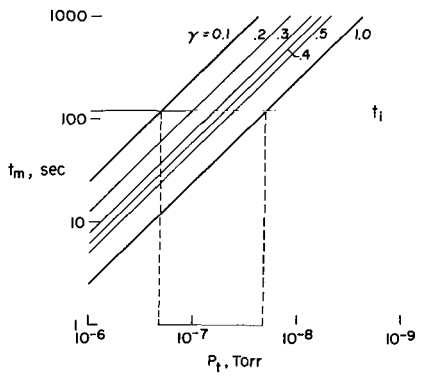

Figure 3.- Dependence of time for monolayer formation on the residual pressure of a gas with a sticking coefficient γ.

The crystallographic structure of the deposit was monitored and recorded at will during deposition by means of selected-area electron diffraction, one of the valuable assets of the in situ electron microscopy technique. The additional information so gained during the early stages of deposition on amorphous substrates usually referred only to the phase of the deposited material. The size of crystallites in very fine and in coarse crystalline overgrowths was determined, in most cases of low supersaturations, directly through the electron microscope image, rather than through diffraction methods as in scanning electron diffraction (ref. 22). Electron diffraction patterns were monitored as a routine procedure. No important deviations from the results of Komnik (ref. 23) were noticed for bismuth, which always nucleated in the liquid phase for substrate temperatures $T \geq 370^{\circ}$ K = 0.68 $\times$ T_m(Bi). Silver invariably condensed in the solid phase, up to the highest substrate temperatures investigated for this material (840° K). However, at high substrate temperatures it is progressively harder to monitor the electron diffraction patterns because of the strongly decreasing number and increasing size of the growing crystallites. (Gladkich and Niedermayer (ref. 24) found silver depositing in the liquid phase at temperatures between about 835° and 935° K.)

RESULTS AND DISCUSSION

Time Dependence of the Number Density of Deposit Particles

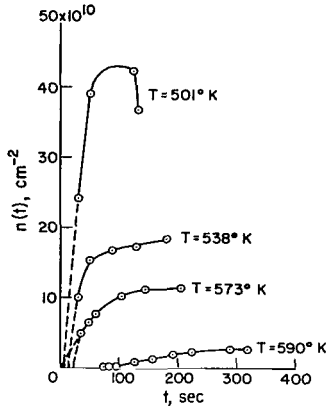

Figure 4.- Time dependence of number density of bismuth nuclei on an evaporated carbon substrate for different T; $\tilde{N} = 1.67 \times 10^{14}$ cm^{-2} sec^{-1}.

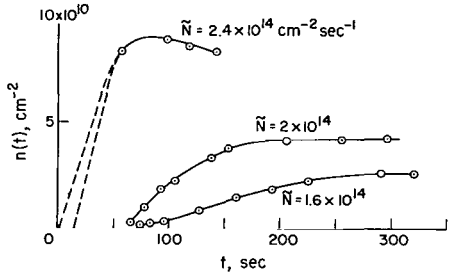

Figure 5.- Time dependence of number density of bismuth nuclei on an evaporated carbon substrate for different N; T = 590° K.

Figures 4 and 5 are typical results obtained by evaluating electron micrographs of thin deposits. The number density n of deposit particles is shown as a function of deposition time, substrate temperature, and impingement flux N of the depositing species. Obvious features of these nucleation curves, and those of other overgrowth-substrate combinations, include the slope of the curves in the steady-state nucleation region, which constitutes the steady-state nucleation rate I; the maximum number density of growing nuclei n_{max} that can be accommodated on a substrate; and the induction time t^o before appreciable nucleation is noticeable. As can be seen qualitatively (figs. 4 and 5), I and n_{max} increase and t^o decreases with rising supersaturation, that is, with falling substrate temperature T and/or increasing impinging flux N. A detailed quantitative discussion of these trends will show that definite conclusions can be drawn concerning such nucleation parameters as ΔG_{des}, n^*, a_o, n_o, and others.

Analysis of Nucleation Rate Measurements by the Atomistic Theory

According to Walton's statistical theory of condensation from the vapor phase, the nucleation rate I is given by the expression:

$$I = Na_o^2 n_o \left(\frac{N}{\omega n_o}\right)^{n^*} \exp\left\{\frac{1}{kT}\left[(n^* + 1)\Delta G_{des} + E_{n^*} - \Delta G_{sd}\right]\right\} \qquad (1)$$

Therefore, the T-dependence of the nucleation rate is

$$\left.\begin{aligned} \log I &= A(n^*, N, n_o, a_o) + B(n^*, \Delta G_{des}, \Delta G_{sd}, E_{n^*}) \frac{1000}{T} \\ A &= (n^* + 1)\log N - n^* \log \omega + 2 \log a_o - (n^* - 1)\log n_o \\ B &= \frac{(n^* + 1)\Delta G_{des} + E_{n^*} - \Delta G_{sd}}{4.58} \end{aligned}\right\} \quad (2)$$

if the respective energies are measured in kcal/mole. The relationship between log I and 1000/T is linear if the impingement flux N is held constant and the parameters n_o, a_o, n^* do not change within a certain temperature interval.

Figure 6 is a schematic plot based upon equations (2), of the type of graph used to evaluate a large number of experimental results quickly. The values for $A^{min}_{n^*}$ correspond to the highest possible number of nucleation sites on a substrate, which is approximately equal to the number of atoms in the substrate surface. A straight line of appropriate slope from the family of curves shown on the graph is first selected so that some of the experimental data points are approximated adequately by a parallel displacement of this line. The families of curves of varying n^* originate at A_1, A_2^{min}, A_3^{min}, etc., and only those straight lines can be chosen that have to be displaced parallel toward higher log I values in order to coincide with the data points. Then the family of curves originating at $A^{min}_{n^*}$ determines n^*; the slope of the line selected marks (B_{n^*}); and the necessary parallel displacement defines A_{n^*} (and therefore $a_o^2/n_o^{n^*-1}$). Only for $n^* = 1$ is it possible to determine directly ΔG_{des} and the length of a single diffusion jump a_o, since $E_1 = 0$ and $\Delta G_{sd} \ll \Delta G_{des}$ (ref. 25). If only a part of the data points can be represented by an $n^* = 1$ line, and a higher n^* curve is indicated for higher substrate temperatures, then the knowledge of ΔG_{des} can be used to calculate E_{n^*} for $n^* > 1$. There is generally more than one choice of n^* (fig. 6). However, the lowest possible n^* value is usually the one to select, since higher values lead to unrealistically high corresponding A_{n^*} values. The selection of n^* and $(a_o^2/n_o^{n^*-1})$ by this method is therefore unique.

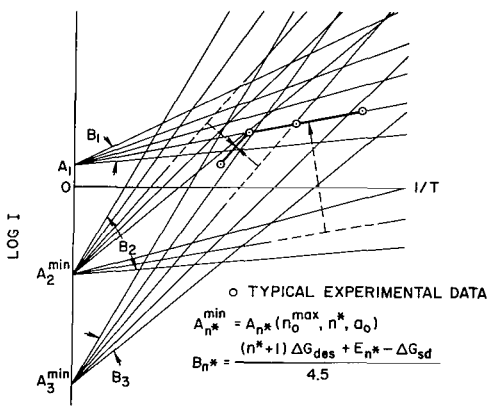

Figure 6.- Schematic graph used for evaluating nucleation rate data.

The nucleation rates for Bi on amorphous carbon (from fig. 4) and for Bi on evaporated SiO are plotted in figures 7 and 8 as a function of reciprocal substrate temperature. The relatively large measurement errors indicated are due to the uncertainties regarding the respective induction times at the start of nucleation. Although straight lines were drawn through the data points, the results for Bi on SiO might better be represented by a curve of steadily

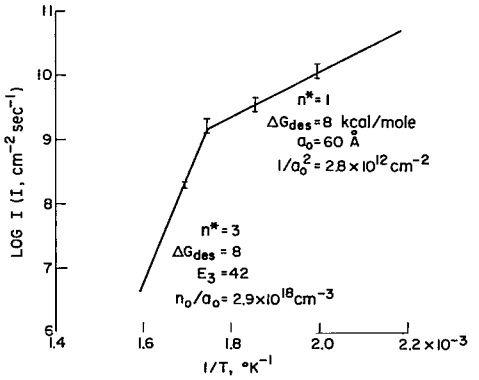

Figure 7.- Temperature dependence of I for bismuth on evaporated carbon (atomistic theory); $\tilde{N} = 1.67\times10^{14}$ cm^{-2} sec^{-1}

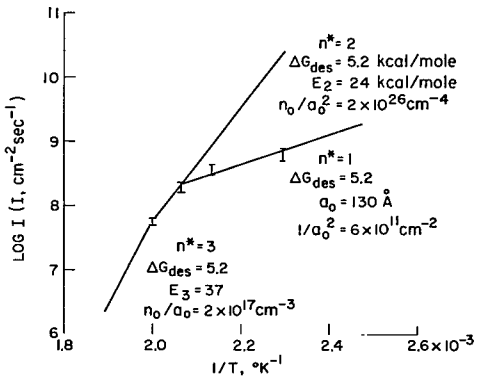

Figure 8.- Temperature dependence of I for bismuth on evaporated SiO (atomistic theory); $\tilde{N} = 7.6\times10^{14}$ cm^{-2} sec^{-1}.

changing curvature. Nucleation parameters pertaining to these lines were determined by following the procedure outlined previously. This analysis shows that a single atom has to be regarded as the critical nucleus for both substrates at lower substrate temperatures. The free energy of desorption ΔG_{des} is 5.2 or 8 kcal/mole for the two substrates. At higher T, the critical size of the nucleus is probably given by $n^* = 3$ for both cases, since the energy E_3 required to dissociate a critical Bi nucleus is 42 and 37 kcal/mole. The surface diffusion jump distances of $a_o(C) = 60$ Å and $a_o(SiO) = 130$ Å derived from the $n^* = 1$ branches (figs. 7 and 8) seem high, and the values of $n_o(C) \simeq 2\times10^{12}$ cm^{-2} and $n_o(SiO) \simeq 3\times10^{11}$ cm^{-2} for the nucleation site densities that result from the respective n_o/a_o ratios of the $n^* = 3$ branches appear low. The combined results for the nucleation of Bi indicate a much smaller nucleation potency of the SiO substrate as compared to the carbon substrate, which can be expected. Because of decreased nucleation potency, the induction times measured for Bi on SiO were two to three times those encountered during Bi on C nucleation.

By rearranging the basic nucleation rate (Eq. (1)), one obtains the following form

$$\left.\begin{aligned} \log I &= C(n^*,T,\Delta G_{des},\Delta G_{sd},n_o,a_o) + (n^* + 1)\log \tilde{N} \\ C &= \frac{(n^* + 1)\Delta G_{des} + E_{n^*} - \Delta G_{sd}}{4.58}\,\frac{1000}{T} - n^* \log \omega + (1 - n^*)\log n_o \\ &\quad + 2 \log a_o \end{aligned}\right\} \qquad (3)$$

which can be used to test the impingement rate dependence of the nucleation rate for constant substrate temperature (fig. 5) when statistical theory is applied. The constant C depends complexly upon a variety of nucleation parameters. However, the slope of the straight line in a log I over log N plot should be equal to $(n^* + 1)$. The solid line (fig. 9) for $n^* = 3$ was calculated with the nucleation parameters obtained from the high-temperature branch of figure 7. The experimentally measured nucleation rate dependence

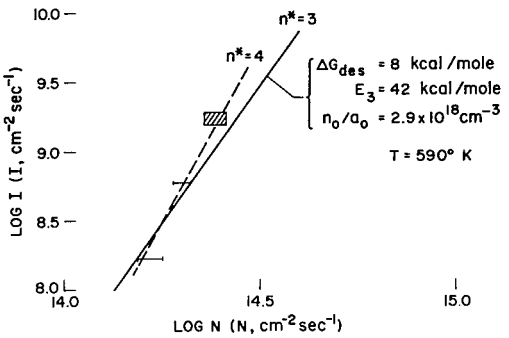

Figure 9.- N-dependence of I for bismuth on evaporated carbon (atomistic theory).

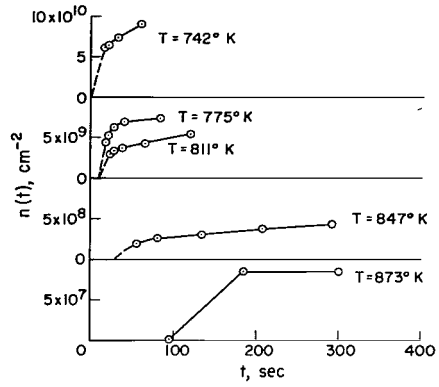

Figure 10.- Time dependence of number density of silver nuclei on evaporated carbon for different T; $\tilde{N} = 6.3 \times 10^{13}$ cm^{-2} sec^{-1}.

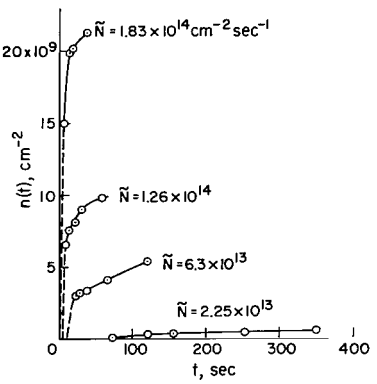

Figure 11.- Time dependence of number density of silver nuclei on evaporated carbon for different N; T = 811° K.

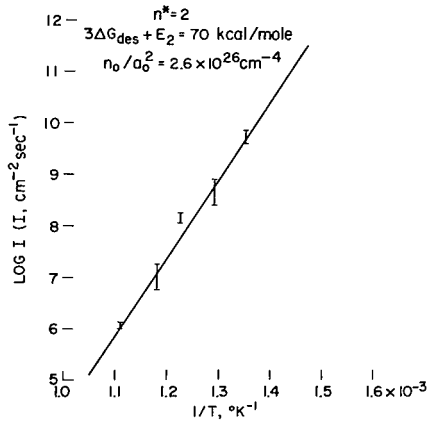

Figure 12.- Nucleation rate of silver on evaporated carbon for different T (atomistic theory); $\tilde{N} = 6.3 \times 10^{13}$ cm^{-2} sec^{-1}.

(fig. 9) is then only roughly approximated by the calculated curve, and a higher value of n^* is indicated.

In principle, the same experiments and theoretical evaluations as described for Bi were performed with silver as the nucleating material. The variation of $n(t)$ as a function of substrate temperature T and impinging flux N is shown (figs. 10 and 11) for the deposition of Ag onto evaporated amorphous carbon. The resulting temperature dependence of the nucleation rate (fig. 12) could not be matched, however, by an $n^* = 1$ curve, which made impossible the direct calculation of ΔG_{des} and a_o. It can be stated only that $\Delta G_{des}(Ag)$ must be smaller than approximately 23 kcal/mole, (otherwise, $E_2 < 0$). If $\Delta G_{des}(Ag)$ is assumed equal to 10 to 12 kcal/mole, on the basis of the same experiments evaluated by means of the phenomenological theoretical concepts, then E_2 equals 35 to 40 kcal/mole (fig. 12) for the dissociation energy of the critical nucleus containing two atoms. This value compares favorably with 38.5 kcal/mole for the binding energy of a diatomic silver molecule (ref. 26). Results correlating I and N for Ag on C are presented in figure 13. The

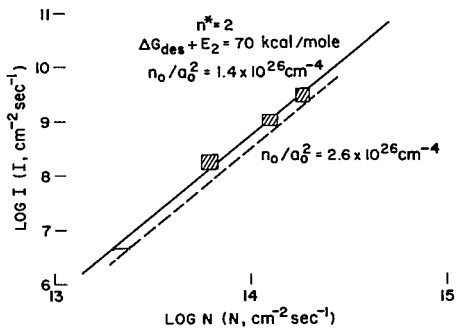

Figure 13.- Nucleation rate of silver on evaporated carbon for different N (atomistic theory); T = 811° K.

dashed line was calculated with the nucleation parameters derived from figure 12. The agreement with the experimental measurements can be improved if a smaller value is used for n_o/a_o^2. This correction results in the solid curve in figure 13.

Analysis of Nucleation Rate Measurements by the Classical Theory

The classical phenomenological theory of references 1 and 2 can be used to interpret the same experimental results of the heterogeneous nucleation of Bi and Ag. In the notation of reference 4 the nucleation rate I is

$$\left.\begin{aligned} I &= C_1 p^2 \exp\left[\frac{1}{kT}\left(2\,\Delta G_{des} - \Delta G_{sd} - \Delta G^*\right)\right] \\ C_1 &= \frac{a_o \sin\theta}{4\pi\omega m}\, l n \,\frac{p}{p_e}\sqrt{\frac{\varphi_3}{kT\sigma}} \\ \Delta G^* &= \frac{16\pi\varphi_3\Omega^2}{3[kT\, l n(p/p_e)]^2}\,\sigma^3 \\ p &= N\sqrt{2\pi m k T}\;;\quad \sigma = \frac{\sigma_B}{l} \end{aligned}\right\} \qquad (4)$$

The additional dimensionless parameter l was introduced here into equations (4) to better match the experimental results with the predictions of the equation.[3]

To calculate the nucleation rate I as a function of T and N, reasonable numerical assumptions (table I) must be made concerning some of the parameters in equations (4). A temperature independent value of $\omega = \text{const} = 10^{13}\ \text{sec}^{-1}$ was taken as surface vibration frequency; the respective bulk surface tensions were introduced; and the equilibrium vapor pressures of Ag and Bi were obtained from reference 28. The choice of a_o

[3]From a theoretical point of view, l can possibly be related to the correction factor $[1 + (2\delta/r)]$ derived by Tolman (ref. 27) from thermodynamic considerations in an attempt to account for the effect of surface curvature on surface tension. The parameter δ is expected to be of the order of 10^{-8} cm; thus, for a nucleus with a 1 Å radius, a value of $[1 + (2\delta/r)] = 3$ would follow formally. But the intrinsic difficulty of Tolman's treatment must be remembered: Tolman assumes a continuous medium, but the surface tension is not appreciably affected until curvatures comparable to atomic dimensions are reached.

TABLE I. NUCLEATION PARAMETERS

	Ag	Bi
m	1.8×10^{-22} g	1.57×10^{-22} g
σ_B	960 erg/cm^2	380 erg/cm^2
p_e	$10^{8.865-\frac{14058}{T}}$ Torr	$10^{7.213-\frac{8397}{T}}$ Torr
a_o	2 Å ; $\theta \approx 65°$	2 Å ; $\theta \approx 90°$
ω	10^{13} sec^{-1}	10^{13} sec^{-1}
Ω	1.715×10^{-23} cm^3	3.54×10^{-23} cm^3

and the contact angle θ was not critical for the present calculations, as can be seen from equations (4) and the fact that

$$\varphi_3 = \frac{2 - 3\cos\theta + \cos^3\theta}{4}$$

φ_3 therefore assumes values from 0.2 to 0.5 when θ changes from 65° to 90°. The actual selections of $\theta(\mathrm{Ag}) = 65°$ and $\theta(\mathrm{Bi}) = 90°$ constitute rough estimates, only, however, on the basis of qualitative considerations of the image contrast of nuclei on corresponding electron micrographs. Although the contact angle of individual nuclei should be measured directly, an intrinsic difficulty of high-resolution transmission electron microscopy - information on the third dimension of small objects - intervenes. A quick determination of small nuclei cross sections appears feasible only when nuclei deposit, and grow, at substrate foil edges so as to make transmission microscopy possible with the imaging electron beam parallel to the substrate surface. The surface diffusion jump distance $a_o = 2$ Å was chosen because the distance of carbon atoms in a graphite surface is of that order.

With the numerical values from table I and the abbreviations,

$$2\,\Delta G_{des} - \Delta G_{sd} = Z\,\frac{\text{kcal}}{\text{mole}}\,; \qquad N = 10^m\ \text{cm}^{-2}\ \text{sec}^{-1} \tag{5}$$

the following expressions for the nucleation rates are obtained from equations (4). For Ag,

$$I = 6.6\,\Phi\sqrt{\ell T}\,N^2\,10^{\frac{218}{T}Z - \frac{1.44\times10^{11}}{(\ell T)^3\Phi^2} - 31} \tag{6a}$$

with

$$\ell n\,\frac{p}{p_e} = \Phi = -69.9 + 2.3m + \frac{1}{2}\,\ell n\,T + \frac{32{,}400}{T}$$

For Bi,

$$I = 7.4\,\Phi\sqrt{\ell T}\,N^2\,10^{\frac{218}{T}Z - \frac{0.95\times10^{11}}{(\ell T)^3\Phi^2} - 31} \tag{6b}$$

with

$$\ell n\,\frac{p}{p_e} = \Phi = -65.8 + 2.3m + \frac{1}{2}\,\ell n\,T + \frac{19{,}350}{T}$$

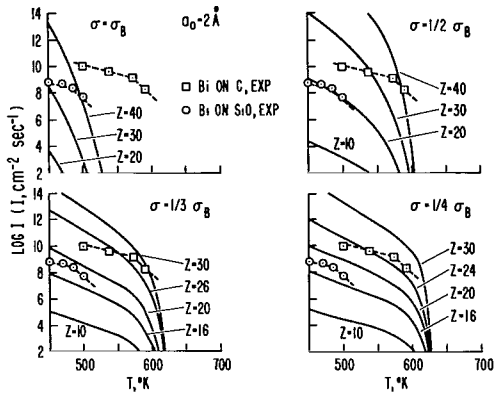

(a) Deposition of bismuth on carbon, and on SiO, $\tilde{N} = 1.67 \times 10^{14}$ cm^{-2} sec^{-1}.

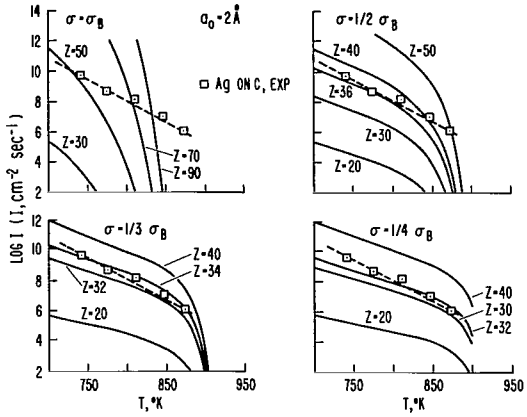

(b) Deposition of silver on carbon, $\tilde{N} = 6.3 \times 10^{13}$ cm^{-2} sec^{-1}.

Figure 14.- Comparison of calculated and experimental nucleation rates (classical theory).

Figures 14 and 15 show the results of evaluating equations (6a) and (6b) with a computer. The solid curves represent the computed nucleation rates; the experimentally measured nucleation rates are connected by dashed lines, which indicate the results of the previous calculations based on the statistical theoretical approach. In figures 14(a) and (b) the impingement rate $\tilde{N}$ was kept constant and the substrate temperature T, the free energy of desorption $\Delta G_{des} \simeq 1/2\ Z$ kcal/mole, and the Tolman factor l ($\sigma = \sigma_B/l$) were varied; whereas in figures 15(a) and (b) T was held constant and $\tilde{N}$, Z, and l were varied.

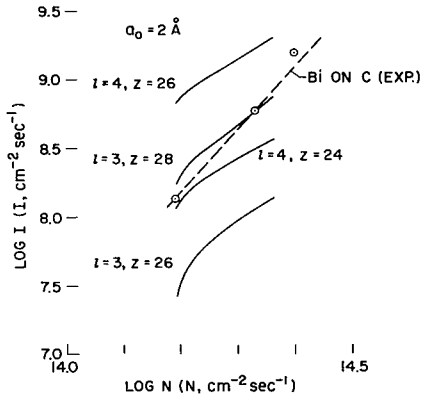

(a) Deposition of bismuth on carbon, T = 590° K.

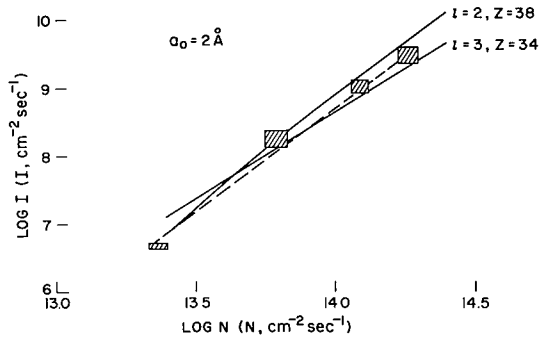

(b) Deposition of silver on carbon, T = 811° K.

Figure 15.- Comparison of calculated and experimental nucleation rates (classical theory).

The reason for introducing the parameter l is obvious when the four graphs of figure 14 that correspond to $l = 1, 2, 3$, and 4 are compared. The representation of the experimental measurements by the calculated curves improves with increasing l, as does the definition of a critical substrate temperature above which nucleation stops. If the free energy of surface diffusion ΔG_{sd} is neglected, desorption energies of $\Delta G_{des} = 11.5 \rightarrow 14$ kcal/mole are deduced for $l = 3$ or 4 in the case of nucleation of Bi on C, while for Bi on SiO, it is found that $\Delta G_{des} \simeq 9$ kcal/mole for $l = 3$ or 4. Although these desorption energies are about 1.7 times higher than the respective values

obtained with the atomistic treatment, the trend to higher desorption energies is confirmed by the differences in the results for the C substrates. What the necessary increase in l from the classical value of $l = 1$ to $l = 3$ or 4 implies, in terms of the size of the critical nucleus, will be discussed in the next paragraph. The improved fit of experiment and theory for higher l is demonstrated even better for the case of Ag on C (fig. 14). An almost perfect fit is obtained here for $l = 3$ with an accompanying energy of desorption of $\Delta G_{des}(Ag) = 17$ kcal/mole. (This value previously led to the assumption $\Delta G_{des}(Ag) = 10$ kcal/mole for the statistical treatment by applying the ratio of 1.7.) The agreement of experiment with the phenomenological theory is also satisfactory as far as the nucleation rate dependence upon the impingement flux is concerned. This can be seen in figures 15(a) and (b), and when the respective l and Z values are compared with those found from the T-dependence of the nucleation rate.

In Walton's statistical theory of condensation, the number of atoms, n^*, in the critical nucleus appeared as a simple explicit parameter in the nucleation rate equation; no assumptions regarding the geometrical shape of the critical nucleus had to be made. The classical theory, however, is based upon ascribing macroscopic thermodynamic properties to nuclei of definite geometrical shapes. This is controversial when nuclei of atomic or near-atomic dimensions are involved. The classical theory has often worked surprisingly well despite this basic shortcoming. The following information about n^* can be deduced from the nucleation results:

The term n^* is defined in the classical theory by

$$n^*\Omega = \alpha \frac{2}{3} \pi (r^*)^3 \tag{7}$$

and with the Gibbs-Thomson equation

$$r^* = \frac{2\sigma\Omega}{kT \ln(p/p_e)} \tag{8}$$

n^* is given by the expression

$$n^* = \alpha \frac{16\pi\sigma^3\Omega^2}{3(kT\Phi)^3} = \begin{cases} \frac{\alpha}{\varphi_3} \frac{3.3\times10^{11}}{(T\Phi l)^3} & \text{for Ag} \\ \\ \frac{\alpha}{\varphi_3} \frac{2.2\times10^{11}}{(T\Phi l)^3} & \text{for Bi} \end{cases} \tag{9}$$

Here the factor α is introduced to account for the geometrical shape of the nucleus; $\alpha/\varphi_3 = 4$ roughly describes a cap-shaped nucleus of hemispherical geometry. Very high apparent supersaturations of the order of 10^{39} (ref. 12), for the heterogeneous nucleation of Ag on Wo field emitter tips, lead to unrealistically low values for n^* according the equation (8). However, the

p/p_e values found now are much smaller and range from 7 to 2×10^4 and 3×10^6 for Ag and Bi, respectively, suggesting more realistic n^* values. For a nucleating material of given equilibrium vapor pressure and impingement flux, equation (9) is of the form $n^* = n^*(T, l, \alpha)$. The corresponding graphs for Bi and Ag are shown in figures 16(a) and (b). These graphs apply strictly to these nucleation experiments only if the experimental results can be represented accurately by the calculated nucleation rate curves of figures 14(a) and (b). The size of the critical nucleus decreases sharply with substrate temperature, and n^* would vary from three to several hundred in the range of deposition temperatures were it not for the necessity that $l > 1$. For Ag on C, the data points were fitted almost perfectly by one of the $l = 3$ family of I(T) curves, which leads to $n^* = 1/2 \rightarrow 11$ (fig. 16(b)). The situation is similar for the other substrate overgrowth combinations, but distinctly too low n^* values result for lower substrate temperatures. This is not surprising because the approximation of experimental measurements by the calculated curves in figures 14(a) and (b) becomes increasingly inaccurate with decreasing T.

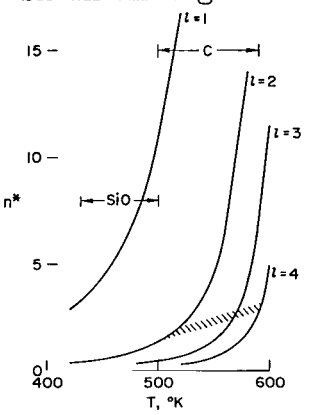

(a) Nucleation of bismuth, $\tilde{N} = 1.67\times10^{14}$ cm^{-2} sec^{-1}, $\alpha/\varphi_3 = 4$.

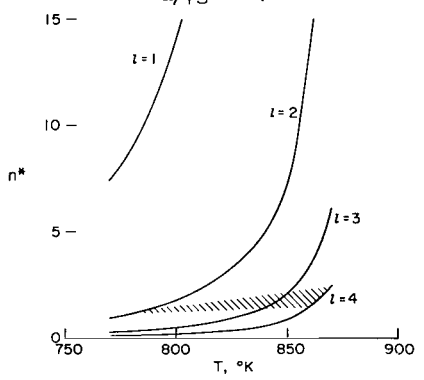

(b) Nucleation of silver, $\tilde{N} = 6.3\times10^{13}$ cm^{-2} sec^{-1}, $\alpha/\varphi_3 = 4$.

Figure 16.- Number of atoms in the critical nucleus for different T and l.

An assumption that the nucleation process is better characterized by the dashed lines in figures 14(a) and (b) results in a different estimate of critical nucleus size. From a comparison of the slope of the dashed straight lines for Bi and Ag on C with those of the curves calculated for various values of l, it is possible to derive a crude dependence of l on T. When the relationship $l = l(T)$ is incorporated in figures 16(a) and (b), nearly constant values for n^* (hatched areas) are obtained: $n^*(Ag) \simeq 1 \rightarrow 2$ and $n^*(Bi) \simeq 2 \rightarrow 3$. The results then compare favorably with the conclusions regarding the size of the critical nucleus drawn earlier from the statistical treatment of the deposition process.

Although justification of the previous conclusions about the size of the critical nucleus remains open for discussion, the trend toward n^* values smaller than the lower limit for classical theoretical concepts seems clear. Recently, Bauer et al. (ref. 29) reached similar conclusions regarding the critical nucleus size when they used the capillarity model in an attempt to analyze the difference in the number of condensed atoms and nucleation rates on alkali halide surfaces with different surface conditions (cleavage in air

as opposed to cleavage in UHV). They estimated that the critical nucleus consists of 5 to 10 metal atoms, confirming the trend to smaller nucleus sizes.

Statistical Mechanical Corrections to the Classical Nucleation Rate Equation

Rodebush (ref. 30) and Lothe and Pound (ref. 31) have modified the classical theory with respect to the absolute entropy of embryos or nuclei. The ensuing statistical mechanical contributions to the free energy of formation of critical nuclei resulted in considerable and still controversial discrepancies of the order of 10^{17} between homogeneous nucleation rates computed with or without these corrections (ref. 4). However, interpretation of heterogeneous nucleation of mercury on quartz-glass (ref. 10), cadmium on copper (ref. 8), and sodium on CsCl (ref. 9) shows (ref. 4) that these results can be described better by corrected nucleation rate expressions. Consequently, the effect of using corrected rate equations to describe our experiments was of interest. The results of the application of corrected rate equations were quite disappointing (see appendix A for details). The so calculated nucleation rates are much too high, indicating the existence of the same dilemma as in the case of homogeneous nucleation.

The Maximum Number Density of Nuclei

The area of surface diffusion, d_s^2, of a randomly migrating adatom is given by the Einstein relationship

$$d_s^2 = \tau a_o^2 2\omega \exp\left(-\frac{\Delta G_{sd}}{kT}\right) \tag{10}$$

where τ is the time of diffusion. The value of τ is determined either by the residence time on the surface before re-evaporation occurs or by the average time before collision with a growing or critical nucleus. In the latter, τ will depend upon the kinetics of nucleation, that is, on the experimental parameters that determine the nucleation rate. If each nucleus or growing cluster is considered surrounded by a "capture area" or "sink zone," d_s^2, then the maximum number of nuclei is, on the average,

$$n_{max} = \frac{1}{d_s^2} = \frac{\exp\left(\frac{\Delta G_{sd}}{kT}\right)}{\tau a_o^2 2\omega} \tag{11}$$

Equation (11) yields a linear dependence of $\log n_{max}$ on $1/T$ only if $\tau = \text{const}$. When T or N or both are varied only over small intervals, this condition can be fulfilled approximately. Walton et al. (ref. 13) and Sumner (ref. 32) measured n_{max} and estimated values for ΔG_{sd} and τ from linear plots of $\log n_{max}$ versus $1/T$. Our experiments and recent results by Chopra (ref. 33), however, show that a linear relationship cannot generally be expected over any appreciable substrate temperature range, and therefore $\tau = \tau(T,N, \ldots)$.

In the interpretation of the experimental results of measurements of the temperature and impingement flux dependence of n_{max} (figs. 3, 4, 9, and 10), the following assumption was made:

$$n_{max} \propto N_{n^*} \tag{12}$$

The number density of critical nuclei on the substrate surface N_{n^*} can be expressed either in terms of Walton's statistical theory of condensation (ref. 14) or those of the phenomenological theory of nucleation. The values for such nucleation parameters as ΔG_{des} and n^* can be deduced, using Walton's approach, and compared with previous results for the same parameters that were obtained through nucleation rate measurements:

$$N_{n^*} = \frac{1}{a_o^2}\left(\frac{Na_o^2}{\omega}\right)^{n^*} \exp\left(\frac{n^*\Delta G_{des} + E_{n^*}}{kT}\right) \tag{13}$$

and therefore with equation (12),

$$\log n_{max} = A(n^*, a_o, \ldots) + n^* \log N + \frac{n^*\Delta G_{des} + E_{n^*}}{4.58}\,\frac{1000}{T} \tag{14}$$

if the respective energies again are measured in kcal/mole. The experimental results for Bi on C are plotted in figure 17. The slopes of the low and high temperature branches correspond to $n^*\Delta G_{des} + E_{n^*} = 10.5$ or 52 kcal/mole, which lead to $\Delta G_{des} = 10.5$ kcal/mole and $E_3 = 20.5$ kcal/mole if $n^* = 1$ applies for low and $n^* = 3$ for higher substrate temperatures. This compares with $\Delta G_{des} = 8$ kcal/mole and $n^* = 1$ for the low T branch of figure 7; for higher temperatures, $n^* = 3$ and $E_3 = 42$ kcal/mole were found in figure 7. Figure 18 presents the impingement flux dependence of n_{max} for the same combination of substrate and deposit material. A linear relationship between $\log n_{max}$ and $1/T$ is expected, according to equation (14). Figure 18 suggests a value of $n^* = 3$ for the high substrate temperature of $T = 590^\circ$ K, in good agreement with previous results.

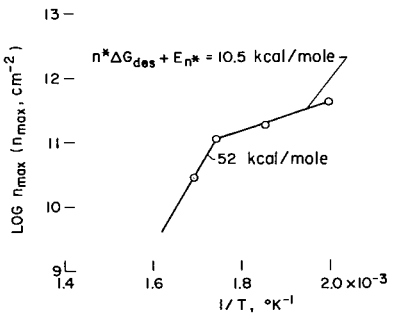

Figure 17.- Temperature dependence of maximum number density of bismuth particles on evaporated carbon; N = 1.6x10^{14} cm^{-2} sec^{-1}.

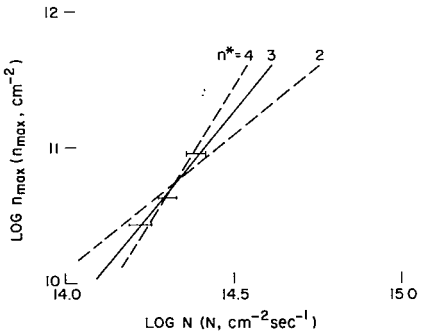

Figure 18.- N-dependence of the maximum number density of bismuth particles; T = 590° K.

The same analysis, in principle, was applied to n_{max} measurements (figs. 10 and 11) for the nucleation of Ag on C; $n^*\Delta G_{des} + E_{n^*} = 57$ kcal/mole summarizes the results of the temperature dependence of n_{max}, and from the slope of the N-dependence curve a value of $n^* = 3$ was deduced. The agreement with previous results (figs. 12 and 13) was again satisfactory.

The n_{max} measurements indicate that the importance of the adatom surface mobility should be reassessed. The surface mobility (ΔG_{sd}) of a depositing material is believed to influence thin-film growth phenomena relating to the maximum number of growing nuclei, n_{max}, but if the previous explanation of n_{max} measurements proves realistic, then (1) the process of adsorption (ΔG_{des}) rather than surface migration (ΔG_{sd}) defines n_{max} and (2) the quantitative determination of ΔG_{sd} is impossible with simple n_{max} measurements. (One should also keep in mind that, usually, ΔG_{sd} is only $(1/5 \rightarrow 1/10)\Delta G_{des}$.)

Induction Times and Growth of Individual Nuclei

During low supersaturation nucleation experiments, a time lag is often observed between the start of deposition and the detection of initial nuclei, a fact shown by the nucleation curves of figures 3, 4, 10, and 11. The time lag t^o (termed the induction time) was found to be due to deficiencies of detection and to the nature of the nucleation process.

Four contributions to the total time lag were considered

$$t^o = t_1 + t_2 + t_3 + t_4$$

Of these four contributions, two (t_1 and t_4) were found to be negligibly small under the present circumstances (see appendix B). Values for the remaining two were calculated in the following manner.

The growth velocity of individual nuclei in conjunction with the resolution capabilities of the detection system must be considered when the time lag contribution t_3 is assessed. The volume growth velocity C_V of a single nucleus can be expressed in different ways, depending upon the assumptions concerning the mechanism of adding material to the nucleus and the state of supersaturation. A formula proposed by Chakraverty (ref. 34)

$$C_V = \frac{dV^o(t)}{dt} = \Omega\pi a_o^2 N \exp\left(\frac{\Delta G_{des} - \Delta G_{sd}}{kT}\right) \qquad (15)$$

is used that applies for low supersaturations and includes material added to the nucleus both by surface migration and direct supply from the vapor phase. The numerical parameters (table I) yield for the case of Bi on C: $C_V \approx 0.8\times10^{-20}$ cm^3 sec^{-1}. Equation (15) can be tested on actual growth velocity measurements for a Bi particle on a carbon substrate (fig. 19). After an unknown shape factor β is introduced, which accounts for only the diameter of nuclei being determined in transmission electron microscopy, it is found

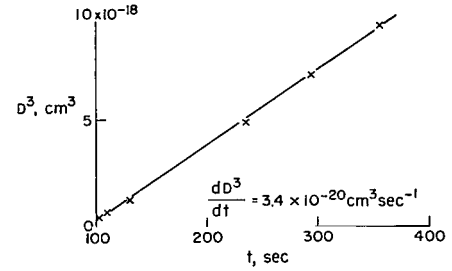

Figure 19.- Growth of an individual bismuth nucleus on carbon.

that $C_v = 3.4\times10^{-20}$ cm^3 sec^{-1} and, therefore, $\beta \simeq 1/4$. This corresponds to a nucleus of approximately semi-spherical shape, a conclusion that is also supported by electron microscope observations of the shape of larger bismuth nuclei.

The minimum size of a detectable nucleus depends on (1) the spatial resolution capability of the detector, (2) the contrast of the small nucleus, and (3) its shape. The smallest detectable nucleus volume is therefore $V^o_{min} = V^o(D_{min}) = \beta D^3_{min}$ and the time lag t_3 can then be written as

$$t_3 = \frac{V^o_{min}}{\pi\Omega a_o^2 \tilde{N}} \exp\left(-\frac{\Delta G_{des} - \Delta G_{sd}}{kT}\right) \qquad (16)$$

and the ratio t_3/β can be plotted as a function of ΔG_{des} and $1/T$ (fig. 20). (The shape factor β depends on the free surface and interfacial energies of the specific substrate and overgrowth materials.) The graph also indicates the substrate temperature intervals covered in various nucleation experiments. The time t_3 is therefore expected to range from seconds (for Ag on C, where $\beta(Ag) < \beta(Bi)$) to tens of seconds (for Bi on C) and even several hundreds of seconds (for Bi on SiO).

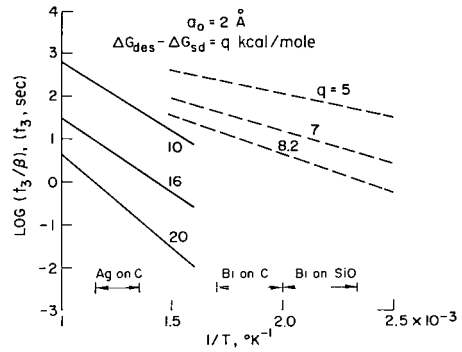

Figure 20.- Time lag for growth of a silver ($\tilde{N} = 6.3\times10^{13}$ cm^{-2} sec^{-1}) or bismuth ($\tilde{N} = 1.7\times10^{14}$ cm^{-2} sec^{-1}) nucleus to $D_{min} = 50$ Å.

Based on Frenkel's conversion of the difference equations governing the kinetics of clustering processes in supersaturated vapors, various expressions (ref. 35) have been deduced for the time lag t_2. Specifically, t_2 must be understood as the time necessary for the nucleation rate I to reach about one-fourth of the steady-state value:

$$t_2 = \frac{4\pi\sigma}{kT\tilde{N}\Phi^2(N,T)} \qquad (17)$$

Here $\Phi = \Phi(T,N, \ldots) = \ln p/p_e = \ln S$, and $\sigma = \sigma_B/l$. The Tolman factor l is expressed by the relationship $l = l(T)$ obtained previously from nucleation rate considerations. Although the absolute value of t_2 according to equation (17) is still undetermined, the trend of the dependence of t_2 on N and T evidently agrees with the experimental time lag observations.

Figures 21(a) and (b) summarize crude observations of the total time lag t^o for Ag and Bi nucleations. For Bi on C (fig. 21(b)), the calculated increase of $(t_3 + t_2) \simeq t^o$ with decreasing supersaturation agrees qualitatively with the observations. A coincidence of t^o (exp) with the calculated t_2 curve can be noted for the deposition of Ag on C (fig. 21(b)). Although this is fortunate, the result could indicate that t_3(Ag) is small, as suggested by previous speculations regarding the time lag contribution t_3.

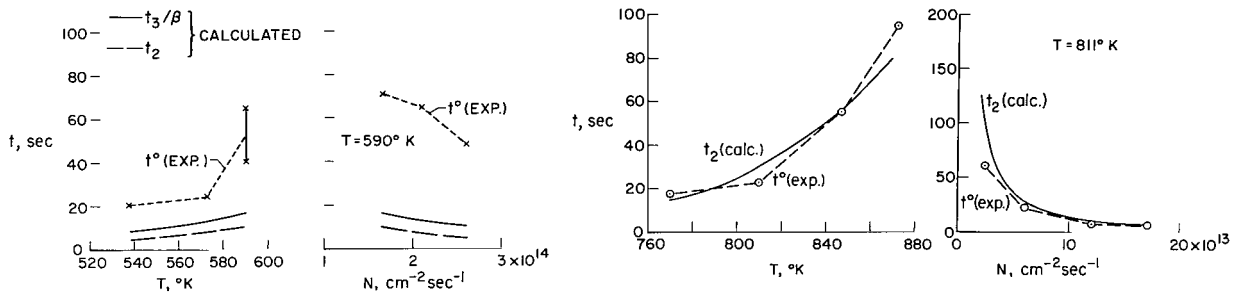

(a) Deposition of bismuth, $\tilde{N} = 6.3\times10^{13}$ cm^{-2} sec^{-1} on evaporated carbon.

(b) Deposition of silver, $\tilde{N} = 6.3\times10^{13}$ cm^{-2} sec^{-1} on evaporated carbon.

Figure 21.- Temperature and impingement flux dependence of t^o.

CONCLUSIONS

1. It is possible to perform controlled quantitative nucleation experiments inside the electron microscope. With the present apparatus, however, it was necessary to limit the studies to a few simple nucleation systems, bismuth and silver on amorphous thin film substrates of evaporated carbon and silicon monoxide. Current developments in the areas of UHV-electron microscope specimen chamber design, electron microscope image intensification, and electronic particle size analysis improve the prospects for investigating less restrictive nucleation systems in the near future.

2. Both the simple capillarity model and the atomistic potential energy model were found useful for the theoretical interpretation of a large part of the present heterogeneous nucleation results by assigning specific values to such important nucleation parameters as n^*, the number of atoms in the critical nucleus and ΔG_{des}, the free energy of desorption.

3. Neither of the two models is completely adequate. The major inconsistencies were found to be

(a) Rather high values for the single diffusion jump distance a_o when the atomistic theory is applied to low-temperature bismuth nucleation rates.

(b) Rather poor representation of the nucleation-rate temperature dependence by the classical theory for lower substrate temperatures.

(c) Desorption energy values that differed by a factor of approximately 1.7 when classical and atomistic results are compared.

These inconsistencies are attributed to the well-known approximations in both theoretical models (particularly to basic limitations in the phenomenological approach of assigning macroscopic thermodynamic properties to very small nuclei).

4. Incorporation of recently introduced statistical mechanical contributions to the free energy of nucleus formation in the capillarity model resulted in unrealistically high theoretical nucleation rates.

5. The present experimental technique is inadequate for measurements during the very early stages of nucleation. Consequently, the induction time measurements were crude and only approximate agreement between theoretical predictions and experimental results was found. However, the determination of the number densities of growing nuclei in later stages of the nucleation process was accurate. Tentative interpretation of the corresponding results, in terms of nucleation limited surface migration, explains the changing slope of the $\log n_{max}$ versus $1/T$ curve.

6. Future experimental efforts should concentrate particularly on techniques for preparing and maintaining well-defined substrate surfaces, assessing and eventually controlling the effects of the imaging electron beam, and rapidly counting and recording growing nuclei. Technical advances in these areas are needed if a better comparison of experimental results and differing theoretical approaches to the problem of heterogeneous nucleation is to be achieved.

Ames Research Center
National Aeronautics and Space Administration
Moffett Field, Calif., 94035, Dec. 14, 1967
129-03-15-10-00-21

APPENDIX A

STATISTICAL MECHANICAL CORRECTIONS OF CLASSICAL NUCLEATION RATE EQUATIONS

Two major contributions to the free energy of formation of a critical nucleus, ΔG^*, must be considered. The first contribution, ΔG_q, arises from the need to distribute the embryos among the available n_o adsorption sites on the substrate surface: $\Delta G_q = -kt \ln(n_o/n_s)$. This applies as long as $\Delta G_{sd} > kt$ (i.e., the embryos can be regarded as localized). When this is no longer valid, the embryos can be regarded as a two-dimensional gas. Additional translational and rotational degrees of freedom must then be considered. The corresponding contributions to ΔG^* (ΔG_t, ΔG_r) have also been given by Hirth and Pound (ref. 4).

To evaluate the different statistical mechanical correction terms in more detail, the ratios of the corrected nucleation rates I' and the classical nucleation rate I were computed from equations (4). The corrected rates I' can be written in the form

$$I' = C \cdot f(T,Z) \cdot I \tag{18}$$

for constant impinging particle flux N.

The ratio I'/I was computed for three different contributions to the free energy of formation of the critical nucleus:

(1) ΔG_q, for localized embryos that are to be distributed among n_o adsorption sites on the substrate surface,

(2) ΔG_t, for embryos translating freely on the substrate surface, and

(3) $\Delta G_t + \Delta G_r$, for freely translating and rotating embryos.

In all three cases, the respective functions f_q, f_t, and f_{t+r} had the desirable effect of flattening slightly (at low substrate temperature) the nearly linear portion of the nucleation rate versus temperature curves (figs. 13 and 14(a)), so that the general shape of the corrected nucleation rate curves resembled the experimental curves more closely. However, this desirable contribution of the corrections was more than offset by the magnitude of the constants C_q, C_t, and C_{t+r}. For an impingement flux of $N = 10^{14}$ cm^{-2} sec^{-1} and at a substrate temperature of $T = 500^{\circ}$ K, the following approximate values resulted:

$$C_q \cdot f_q \simeq 10^9 \tag{19}$$

for $n_o = 10^{15}$ cm^{-2},

$$C_t \cdot f_t \simeq 10^{11} \tag{20}$$

and

$$C_{t+r} \cdot f_{t+r} \simeq 10^{13} \tag{21}$$

Therefore, the corrected capillarity model of the nucleation process does not seem applicable for our experimental deposition conditions.

APPENDIX B

ESTIMATE OF INDUCTION TIME CONTRIBUTIONS t_1 AND t_4

In the definition of t_1, the induction time had been related to a time-dependent adatom concentration. The corresponding time-dependent supersaturation ratio S is given by

$$S(t) = \frac{N\sqrt{2\pi mkT}}{p_e \tau_s} t \qquad (22)$$

for $t < \tau_s$, where τ_s is the residence time of an adatom on the substrate surface. At $t_1 = \tau_s = (1/\omega)\exp(\Delta G_{des}/kT)$, the steady-state value of S is reached. Figure 22 shows that in all deposition experiments of low adsorption energies τ_s is of the order of 10^{-9} sec, and t_1 can therefore be neglected.

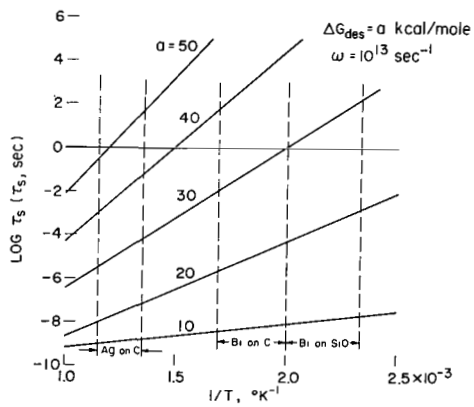

Figure 22.- Residence time of an adatom on the substrate surface.

The time t_4 can be estimated from

$$t_4 = \frac{1}{IF} \qquad (23)$$

where F represents the field of view. When the nucleation process is observed on the viewing screen (6×5 cm^2) of an electron microscope, $F = 1.7\times10^{-8}$ cm^2 for a typical magnification of $\times 40{,}000$. Therefore

$$t_4 = 0.6 \times \frac{10^8}{I} \text{ sec}$$

if I is measured in cm^{-2} sec^{-1}. However, for nucleation rates of 10^8 cm^{-2} sec^{-1} and lower, the field of view can be enlarged readily by continuous scanning of a larger substrate area in the electron microscope; t_4 can then be disregarded.

REFERENCES

1. Volmer, M.; and Weber, A.: Nuclei Formation in Supersaturated States. Z. Physik. Chem., vol. 119, 1926, p. 277.

2. Becker, R.; and Doring, W.: Kinetic Treatment of Grain-Formation in Supersaturated Vapours. Ann. Phys., vol. 24, no. 5, 1935, p. 719.

3. Frenkel, F.: Kinetic Theory of Liquids. Oxford Univ. Press, London, 1947.

4. Hirth, J. P.; and Pound, G. M.: Condensation and Evaporation; Nucleation and Growth Kinetics. The Macmillan Co., N. Y., 1963.

5. Knudsen, M.: Condensation of Metallic Vapours on Cooled Bodies. Ann. Phys., vol. 50, 1916, p. 472.

6. Wood, R. W.: Condensation and Reflection of Gas Molecules. Phil. Mag., vol. 32, 1916, p. 364.

7. Estermann, I.: The Influence of Ray Density and Geometrical Dimensions upon the Formation of Deposits from Molecular Rays. Z. Physik, vol. 33, 1925, p. 320.

8. Cockcroft, J. D.: Phenomena Occurring in the Condensation of Molecular Streams on Surfaces. Proc. Roy. Soc. (London) Ser. 119A, 1928, p. 293.

9. Yang, L.; Birchenall, C. E.; Pound, G. M.; and Simnad, M. T.: Some Observations on Heterogeneous Nucleation of Sodium Crystals from Atomic Beams. Acta Met., vol. 2, 1954, p. 462.

10. Mayer, H.; and Gohre, H.: The Phenomenon of Delayed Condensation. Naturwiss., vol. 49, 1962, p. 253.

11. Moazed, K. L.; and Pound, G. M.: Field-Emission Microscopy of Metal Crystal Nucleation. Trans. Met. Soc. AIME, vol. 230, 1964, p. 234.

12. Gretz, R. D.; and Pound, G. M.: Condensation and Evaporation of Solids. Gordon and Breach, N. Y., 1964.

13. Walton, D.; Rhodin, T. N.; and Collins, R. W.: Nucleation of Silver on Sodium Chloride. J. Chem. Phys., vol. 38, 1963, p. 2698.

14. Walton, D.: Nucleation of Vapor Deposits. J. Chem. Phys., vol. 37, 1962, p. 2182.

15. Poppa, H.: Progress in the Continuous Observation of Thin-Film Nucleation and Growth Processes by Electron Microscopy. J. Vac. Sci. Technol., vol. 2, 1965, p. 42.

16. Bauer, E.; Green, A. K.; Kunz, K. M.; and Poppa, H.: The Formation of Thin Continuous Films from Isolated Nuclei. Basic Problems in Thin Film Physics, Vandenhoeck and Ruprecht (Gottingen), 1966, p. 135.

17. McLauchlan, T. A.; Sennett, R. S.; and Scott, G. D.: Continuous Observation with the Electron Microscope on the Formation of Evaporated Films of Silver, Gold and Tin. Can. J. Res., vol. 28A, 1950, p. 530.

18. Bassett, G. A.: Continuous Observation of the Growth of Vacuum Evaporated Metal Films. Proc. European Regional Conference on Electron Microscopy, Delft, 1960, p. 270.

19. Pashley, D. W.; Stowell, H. J.; Jacobs, M. H.; and Law, T. J.: The Growth and Structure of Gold and Silver Deposits Formed by Evaporation Inside an Electron Microscope. Phil. Mag., 8th ser., vol. 10, 1964, p. 127.

20. Valdre, U.; Pashley, D. W.; Robinson, E. A.; Stowell, M. J.; Routledge, K. J.; and Vincent, R.: An Ultra High Vacuum Specimen Chamber with Facilities for Growing Thin Films. Proc. International Conference on Electron Microscopy, 6th Conference, Kyoto, 1966, p. 155.

21. Grigson, C. W. B.; Nixon, W. C.; and Tothill, F.: An Ultra High Vacuum Transmission Electron Microscope. Proc. International Conference on Electron Microscopy, 6th Conference, Kyoto, 1966, p. 157.

22. Grigson, C. W. B.; and Dove, D. B.: Scanning Electron Diffraction of Film Growth. J. Vac. Sci. Technol., vol. 3, 1966, p. 120.

23. Komnik, Yu. F.; Characteristic Condensation Temperatures of Thin Films. Soviet Phys.-Solid State, vol. 6, 1965, p. 2309.

24. Niedermayer, T.; Gladkich, T. N.; and Spiegel, K.: Evidence of Large Depressions in the Melting Points of Thin Metal Films. Phys. Stat. Sol., vol. 15, 1966, p. 181.

25. Ehrlich, G.: Adsorption on Clean Surfaces. Ann. N. Y. Acad. Sci., vol. 101, 1963, p. 722.

26. Ackermann, M.; Stofford, F. E.; and Drowart, J.: Mass-Spectrometric Determination of the Dissociation Energies of the Molecules AgAu, AgCu, and AuCu. J. Chem. Phys., vol. 33, 1960, p. 1784.

27. Tolman, R. C.: The Effect of Droplet Size on Surface Tension. J. Chem. Phys., vol. 17, 1949, p. 333.

28. Nesjemanov, An. N.: Vapor Pressure of the Elements. Academic Press, 1963.

29. Bauer, E.; and Green, A. K.: On the Formation of Single Crystal Films of Face-Centered Cubic Metals on Alkali Halide Cleavage Planes. 2nd Quarterly Status Report, NASA Contract R-05-030-001, July, 1966. Kunz, K. M., Green, A. K., and Bauer, E.: On the Formation of Single Crystal Films of Face Centered Cubic Metals on Alkali Halide Cleavage Planes in Ultra-High Vacuum. Phys. Stat. Sol., vol. 18, 1966, p. 441.

30. Rodebush, W. H.: Nuclei in Evaporation and Condensation. Chem. Rev., vol. 44, 1949, p. 269.

31. Lothe, J.; and Pound, G. M.: Reconsiderations of Nucleation Theory. J. Chem. Phys., vol. 36, 1962, p. 2080.

32. Sumner, G. G.: Effects of Substrate Temperature on the Growth of Thin Platinum Deposits on Rock Salt. Phil. Mag., vol. 12, 8th ser., 1965, p. 767.

33. Chopra, K. L.: Growth of Sputtered vs. Evaporated Films. J. Appl. Phys., vol. 37, 1966, p. 3405.

34. Chakraverty, B. K.: Kinetics of Nucleation Processes. Basic Problems in Thin Film Physics, Vandenhoeck and Ruprecht (Gottingen), 1966, p. 43.

35. Courtney, W. G.: Non-Steady-State Nucleation. J. Chem. Phys., vol. 36, 1962, p. 2009.

NASA-Langley, 1968 — 24 A-2544

"The aeronautical and space activities of the United States shall be conducted so as to contribute . . . to the expansion of human knowledge of phenomena in the atmosphere and space. The Administration shall provide for the widest practicable and appropriate dissemination of information concerning its activities and the results thereof."

—NATIONAL AERONAUTICS AND SPACE ACT OF 1958

NASA SCIENTIFIC AND TECHNICAL PUBLICATIONS

TECHNICAL REPORTS: Scientific and technical information considered important, complete, and a lasting contribution to existing knowledge.

TECHNICAL NOTES: Information less broad in scope but nevertheless of importance as a contribution to existing knowledge.

TECHNICAL MEMORANDUMS: Information receiving limited distribution because of preliminary data, security classification, or other reasons.

CONTRACTOR REPORTS: Scientific and technical information generated under a NASA contract or grant and considered an important contribution to existing knowledge.

TECHNICAL TRANSLATIONS: Information published in a foreign language considered to merit NASA distribution in English.

SPECIAL PUBLICATIONS: Information derived from or of value to NASA activities. Publications include conference proceedings, monographs, data compilations, handbooks, sourcebooks, and special bibliographies.

TECHNOLOGY UTILIZATION PUBLICATIONS: Information on technology used by NASA that may be of particular interest in commercial and other non-aerospace applications. Publications include Tech Briefs, Technology Utilization Reports and Notes, and Technology Surveys.

Details on the availability of these publications may be obtained from:

SCIENTIFIC AND TECHNICAL INFORMATION DIVISION

NATIONAL AERONAUTICS AND SPACE ADMINISTRATION

Washington, D.C. 20546